Computer Assisted Mechanics and Engineering Sciences, 4: 453–476, 1997.

Study of a family of hybrid-Trefftz folded plate p-version elements

Jaroslav Jirousek*
LSC, Department of Civil Engineering, Swiss Federal Institute of Technology
1015 Lausanne, Switzerland

Bogdan Szybiński† and Andrzej P. Zieliński‡
Institute of Mechanics and Machine Design, Technical University of Cracow
ul. Warszawska 24, 31–155 Kraków, Poland

(Received December 20, 1996)

The reported research presents a finite element formulation for folded plate analysis based on the p-version of the hybrid-Trefftz finite element model. The internal displacement field of the elements consists of a suitably truncated T-complete set of in-plane (u, v) and out-of-plane (w) components which satisfy the respective governing differential plane elasticity and thin plate (Kirchhoff) equations. Conformity is enforced in a weak, weighted residual sense through an auxiliary displacement frame, independently defined at the boundary of the element and consisting of displacement components $\bar{u}$, $\bar{v}$, $\bar{w}$ and normal rotation $\bar{\varphi} = \bar{w}_n$. The displacement frame parameters are the global Cartesian displacements $\tilde{U}$, $\tilde{V}$, $\tilde{W}$ at corner nodes and the hierarchical side-mode parameters for normal rotation and the global Cartesian displacement components, an optional number of which is allotted, formally, to mid-side nodes. The investigated approach is assessed on numerical examples.

1. Introduction

The hybrid-Trefftz (HT) finite element model [1] is the oldest and most popular version of the so-called T-elements, a class of formulations [2, 3] which attempt to unite the versatility of conventional finite elements with the accuracy and high convergence rate exhibited by the boundary solution (BS) approaches. The common feature of this class of formulations is that the displacement field of the element has to satisfy the governing differential equations of the problem *a priori*, as in the classical Trefftz's method [4], and the interelement continuity and the boundary conditions are then enforced. In the standard HT formulation, these conditions are enforced through an auxiliary displacement frame independently defined at the element boundary in terms of nodal parameters, which are the final unknowns of the problem (exactly as in the case of the conventional assumed displacement FE). The p-version of the HT formulation applied in this paper is concerned with elements of adjustable accuracy exhibiting a fixed number of degrees of freedom (DOF) at element corner nodes and an optional number of hierarchic side-mode DOF allotted for convenience, formally, to mid-side nodes. A detailed assessment of various advantages of such elements over the conventional FE may be found elsewhere [5].

In principle, a HT folded plate p-element may be obtained by coupling the HT plane elasticity [6] and Kirchhoff plate [7] p-elements. However, since the former is based on enforcing the C^0 conformity on the in-plane displacement components u and v, while the latter requires the enforcement of the C^1 conformity on the out-of-plane displacement component w, a difficulty arises at the com-

* Professor

† Research engineer

‡ Assoc. Professor

mon boundary of two not-coplanar elements. Moreover, an additional problem is encountered as a consequence of the assumption of equal normal rotation along the common part of the boundary of two or more assembled elements. This assumption leads to the unjustified vanishing of the in-plane shear strain at any common corner node where three or more not-coplanar elements meet. These problems, inexistent in the case of the Reissner–Mindlin plate bending model, may in the case of the Kirchhoff plate theory be solved only if use is made in the HT element formulation of a suitably modified displacement frame. Here the consideration of the existence of the out-of-plane internal displacement field w and of the corresponding normal rotation $\varphi = \partial w/\partial n$ at the element boundary leads to the conclusion that the normal component $\tilde{\varphi}$ of the frame may be rendered independent of the out-of-plane displacement component $\tilde{w}$ of the frame. This in turn makes it possible to use for $\tilde{w}$ the same interpolation as for the in-plane components $\tilde{u}$ and $\tilde{v}$ and thus solve the conflict between the C^0 and C^1 conformity requirements at the element boundary as well as the problem of representation of the in-plane shear at corner nodes where three or more not-coplanar elements meet.

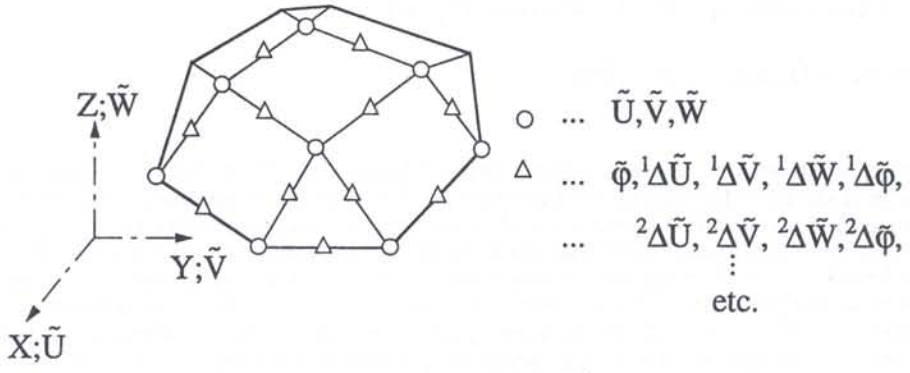

Fig. 1. Typical mesh of HT folded plate p-elements

The above outlined approach is presented in detail in the next section. This approach makes it possible to generate the folded plate p-elements which after the transformation from the local (x, y, z) to the global Cartesian reference frame (X, Y, Z) possess (Fig. 1) three global Cartesian displacement DOF $\left(\tilde{U}, \tilde{V}, \tilde{W}\right)$ at the element corners and an optional number of hierarchic side-mode DOF for the normal rotation $\tilde{\varphi}$ and the global Cartesian displacement components.

Several numerical examples presented in Section 3 were studied to investigate the reliability, the accuracy, and the h- and p-convergence of the new HT folded plate p-elements. Their advantages and shortcomings are discussed and other concluding remarks are presented in Section 4.

2. Theory

2.1. Short recall of the element approach

An obvious alternative to Rayleigh–Ritz methods as a basis for a finite element (FE) formulation is the class of the so-called T-element formulations [2, 3] initiated in 1978 [1] and associated with the method of Trefftz [4]. The common feature of all T-element approaches (of which now many alternative formulations exist [3]) is the use of a non-conforming element displacement field

$$\mathbf{u} = \mathring{\mathbf{u}} + \sum_{j=1}^{m} \mathbf{M}_j c_j = \mathring{\mathbf{u}} + \mathbf{M}\mathbf{c}\,, \tag{1}$$

where c_j stands for unknown parameters and $\overset{\circ}{\mathbf{u}}$ and $\mathbf{M}_j$ are known functions chosen so that the governing differential equations (and as a consequence the equations of equilibrium and constitutive relations) are satisfied in the element subdomain Ω^e. If these equations are written as

$$\mathcal{L}\mathbf{u} = \bar{\mathbf{b}} \tag{2}$$

($\mathcal{L}$ — linear differential operator matrix, $\bar{\mathbf{b}}$ — term representing the specified load on Ω^e), then the satisfaction of (2) for any value of undetermined parameters c_j implies

$$\mathcal{L}\overset{\circ}{\mathbf{u}} = \bar{\mathbf{b}} \quad \text{and} \quad \mathcal{L}\mathbf{M}_j = 0 \quad \text{on } \Omega^e . \tag{2a,b}$$

From (1) can readily be derived the corresponding conjugate vectors of generalized boundary displacements and boundary tractions,

$$\mathbf{v} = \overset{\circ}{\mathbf{v}} + \mathbf{N}\mathbf{c} \quad \text{and} \quad \mathbf{t} = \overset{\circ}{\mathbf{t}} + \mathbf{T}\mathbf{c} \tag{3a,b}$$

at the element boundary Γ^e. What is left is to determine the parameters $\mathbf{c}$ so as to enforce on $\mathbf{v}$ and $\mathbf{t}$ the following conditions:

- the interelement conformity and the kinematic boundary conditions

$$\mathbf{v}^e = \mathbf{v}^f \text{ on } \Gamma^e \cap \Gamma^f , \quad \mathbf{v}^e = \bar{\mathbf{v}} \text{ on } \Gamma^e \cap \Gamma_v , \tag{4a,b}$$

- the reciprocity and the statical boundary conditions

$$\mathbf{t}^e + \mathbf{t}^f = \mathbf{0} \text{ on } \Gamma^e \cap \Gamma^f , \quad \mathbf{t}^e = \bar{\mathbf{t}} \text{ on } \Gamma^e \cap \Gamma_t , \tag{4c,d}$$

(e and f stand for two neighbouring elements, Γ_v and Γ_t for the supported and the free parts of the domain boundary $\Gamma = \Gamma_v \cup \Gamma_t$, $\bar{\mathbf{v}}$ and $\bar{\mathbf{t}}$ are the imposed quantities).

The most frequently used T-element approach [1, 2, 3] is to link the T-elements through an interface displacement frame surrounding the element and approximated independently of (1) in terms of the same nodal DOF, $\mathbf{d}$, as used in the conventional assumed displacement elements:

$$\tilde{\mathbf{v}} = \tilde{\mathbf{N}}\mathbf{d} \quad \text{on} \quad \Gamma^e = \partial\Omega^e . \tag{5}$$

It is assumed that this auxiliary field is such that at a common portion of the boundary of any two neighbouring elements, e and f,

$$\mathbf{v}^e = \mathbf{v}^f \text{ on } \Gamma^e \cap \Gamma^f . \tag{5a}$$

Then enforcing first in a weak sense the conformity on $\mathbf{u}$

$$\int_{\Gamma^e} \delta\mathbf{t}^{\mathrm{T}} (\mathbf{v} - \tilde{\mathbf{v}}) \, \mathrm{d}\Gamma = 0, \tag{6a}$$

and next using the equivalency of virtual works

$$\delta\mathbf{d}^{\mathrm{T}}\mathbf{r} = \int_{\Gamma^e} \delta\tilde{\mathbf{v}}^{\mathrm{T}}\mathbf{t} \, \mathrm{d}\Gamma - \int_{\Gamma_t^e} \delta\tilde{\mathbf{v}}^{\mathrm{T}}\bar{\mathbf{t}} \, \mathrm{d}\Gamma, \tag{6b}$$

where $\mathbf{r}$ stands for equivalent nodal forces associated with the nodal DOF $\mathbf{d}$, enables one to eliminate the undetermined parameters $\mathbf{c}$ and derive for the element the customary force–displacement relationship

$$\mathbf{r} = \overset{\circ}{\mathbf{r}} + \mathbf{k}\mathbf{d} . \tag{7}$$

The load dependent part $\overset{\circ}{\mathbf{r}}$ of $\mathbf{r}$ and the symmetric positive definite stiffness matrix $\mathbf{k}$ in (7) are readily evaluated (for details see e.g. [2]) as

$$\overset{\circ}{\mathbf{r}} = \mathbf{g} - \mathbf{G}\mathbf{H}^{-1}\mathbf{h} \quad \text{and} \quad \mathbf{k} = \mathbf{G}\mathbf{H}^{-1}\mathbf{G}^{\mathrm{T}}, \tag{7a,b}$$

where

$$\mathbf{H} = \int_{\Gamma^e} \mathbf{T}^{\mathrm{T}}\mathbf{N}\,\mathrm{d}\Gamma = \int_{\Gamma^e} \mathbf{N}^{\mathrm{T}}\mathbf{T}\,\mathrm{d}\Gamma, \quad \mathbf{h} = \int_{\Gamma^e} \mathbf{T}^{\mathrm{T}}\,\overset{\circ}{\mathbf{v}}\,\mathrm{d}\Gamma, \tag{8a,b}$$

$$\mathbf{G} = \int_{\Gamma^e} \tilde{\mathbf{N}}^{\mathrm{T}}\mathbf{T}\,\mathrm{d}\Gamma, \quad \mathbf{g} = \int_{\Gamma^e} \tilde{\mathbf{N}}^{\mathrm{T}}\,\overset{\circ}{\mathbf{t}}\,\mathrm{d}\Gamma - \int_{\Gamma_t^e} \tilde{\mathbf{N}}^{\mathrm{T}}\bar{\mathbf{t}}\,\mathrm{d}\Gamma \tag{8c,d}$$

(note that to obtain a nonsingular matrix $\mathbf{H}$, the homogeneous solutions $\mathbf{M}_j$ in (1) should not contain any rigid body modes [1]). Clearly such elements can be handled exactly as the conventional elements (use of the standard direct stiffness method for the element assembly) and as such be implemented without difficulties into standard FEM codes.

2.2. Application to folded plates

2.2.1. General outline of the approach

If considered in its local Cartesian reference frame (x, y, z) (Fig. 2), the membrane (m) and the plate bending (b) components of the response of a folded plate element may be uncoupled. The general HT element formulation from the preceding subsection is applied in turn to the assumed in-plane

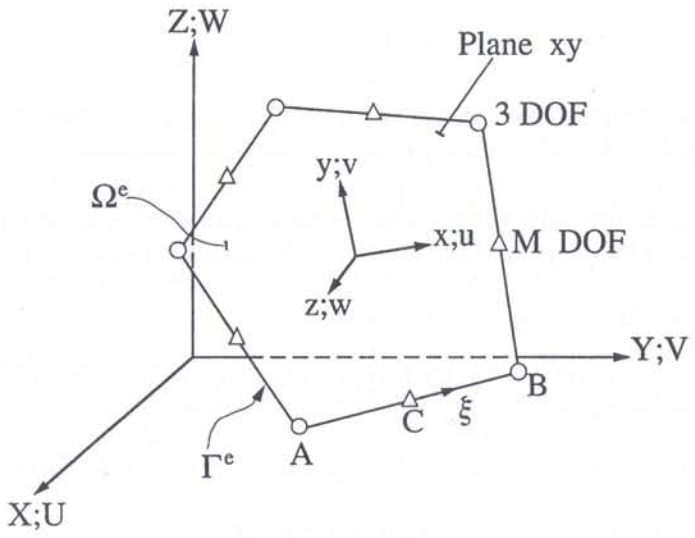

Fig. 2. Typical folded plate HT p-element

and out-of-plane displacements, $\mathbf{u} = \mathbf{u}^{\mathrm{m}} = \{\mathbf{u}, \mathbf{v}\}$ and $\mathbf{u} = \mathbf{u}^{\mathrm{b}} = \{\mathbf{w}\}$, and yields two independent force–displacement relations,

$$\mathbf{r}^{\mathrm{m}} = \overset{\circ}{\mathbf{r}}{}^{\mathrm{m}} + \mathbf{k}^{\mathrm{m}}\mathbf{d}^{\mathrm{m}} \quad \text{(membrane component)}, \tag{9a}$$

$$\mathbf{r}^{\mathrm{b}} = \overset{\circ}{\mathbf{r}}{}^{\mathrm{b}} + \mathbf{k}^{\mathrm{b}}\mathbf{d}^{\mathrm{b}} \quad \text{(plate bending component)} \tag{9b}$$

which may be combined into a single one stated as

$$\mathbf{r} = \begin{Bmatrix} \mathbf{r}^{\mathrm{m}} \\ \mathbf{r}^{\mathrm{b}} \end{Bmatrix} = \begin{Bmatrix} \overset{\circ}{\mathbf{r}}{}^{\mathrm{m}} \\ \overset{\circ}{\mathbf{r}}{}^{\mathrm{b}} \end{Bmatrix} + \begin{bmatrix} \mathbf{k}^{\mathrm{m}} & \mathbf{0} \\ \mathbf{0} & \mathbf{k}^{\mathrm{b}} \end{bmatrix} \begin{Bmatrix} \mathbf{d}^{\mathrm{m}} \\ \mathbf{d}^{\mathrm{b}} \end{Bmatrix} = \overset{\circ}{\mathbf{r}} + \mathbf{k}\mathbf{d}\,. \tag{9c}$$

To allow the standard element assembly to be performed (direct stiffness method), the above relation should then be transformed from the local (x, y, z) to the global (X, Y, Z) reference frame,

$$\mathbf{R} = \overset{\circ}{\mathbf{R}} + \mathbf{KD} \tag{10}$$

by the application of the standard transformation process:

$$\overset{\circ}{\mathbf{R}} = \mathbf{L}^{\mathrm{T}} \overset{\circ}{\mathbf{r}}, \quad \mathbf{K} = \mathbf{L}^{\mathrm{T}} \mathbf{k} \mathbf{L}, \tag{10a,b}$$

where $\mathbf{L}$ stands for the orthogonal transformation matrix (see paragraph 2.2.4) which defines the local DOF in terms of the global DOF of the element:

$$\mathbf{d} = \mathbf{LD}. \tag{10c}$$

2.2.2. Plane elasticity component

Here the internal displacement field has two components

$$\mathbf{u}^{\mathrm{m}} = \begin{Bmatrix} u \\ v \end{Bmatrix}. \tag{11}$$

The conjugate vectors $\mathbf{v}^{\mathrm{m}}$ and $\mathbf{t}^{\mathrm{m}}$ at the element boundary Γ^e have the following definitions

$$\mathbf{v}^{\mathrm{m}} = \begin{Bmatrix} u \\ v \end{Bmatrix}, \quad \mathbf{t}^{\mathrm{m}} = \begin{Bmatrix} t_x^{\mathrm{m}} \\ t_y^{\mathrm{m}} \end{Bmatrix} = \begin{Bmatrix} n_x N_x + n_y N_{xy} \\ n_y N_y + n_x N_{xy} \end{Bmatrix}, \tag{12a,b}$$

where n_x, n_y are direction cosines of the external normal, $\vec{n}$, to element boundary and N_x, N_y, N_{xy} are membrane forces:

$$N_x = \frac{Et}{1-\nu^2}\left(\frac{\partial u}{\partial x} + \nu \frac{\partial v}{\partial y}\right), \tag{13a}$$

$$N_y = \frac{Et}{1-\nu^2}\left(\frac{\partial v}{\partial y} + \nu \frac{\partial u}{\partial x}\right), \tag{13b}$$

$$N_{xy} = \frac{Et}{2(1+\nu)}\left(\frac{\partial u}{\partial y} + \frac{\partial v}{\partial x}\right) \tag{13c}$$

(t — element thickness, E — Young modulus, ν — Poisson's ratio).

The governing differential plane elasticity equations (plane stress assumed) may be explicitly written as

$$\left.\begin{aligned} \frac{Et}{1-\nu^2}\left(\frac{\partial^2 u}{\partial x^2} + \frac{1-\nu}{2}\frac{\partial^2 u}{\partial y^2} + \frac{1+\nu}{2}\frac{\partial^2 v}{\partial x \partial y}\right) &= -\bar{b}_x \\ \frac{Et}{1-\nu^2}\left(\frac{\partial^2 v}{\partial y^2} + \frac{1-\nu}{2}\frac{\partial^2 v}{\partial x^2} + \frac{1+\nu}{2}\frac{\partial^2 u}{\partial x \partial y}\right) &= -\bar{b}_y \end{aligned}\right\}, \tag{14}$$

where $\bar{b}_x$, $\bar{b}_y$ stand for body forces. For $\bar{b}_x = \mathrm{const}$, $\bar{b}_y = \mathrm{const}$, the particular part of the solution may be taken as

$$\overset{\circ}{\mathbf{u}}{}^{\mathrm{m}} = \begin{Bmatrix} \overset{\circ}{u} \\ \overset{\circ}{v} \end{Bmatrix} = \frac{1+\nu}{E} \begin{Bmatrix} \bar{b}_x y^2 \\ \bar{b}_y x^2 \end{Bmatrix} \tag{15}$$

A T-complete set of homogeneous solutions $\mathbf{M}_j^{\mathrm{m}}$ $(j = 1, 2, \ldots)$ may be obtained in a systematic way if one considers in turn the real and the imaginary parts of the four complex functions,

$$\left.\begin{aligned} A_k &= (3-\nu)\,\mathrm{i}\left(\frac{z}{d}\right)^k + (1+\nu)\,k\mathrm{i}\left(\frac{z}{d}\right)\left(\frac{\bar{z}}{d}\right)^{k-1} \\ B_k &= (3-\nu)\left(\frac{z}{d}\right)^k - (1+\nu)\,k\left(\frac{z}{d}\right)\left(\frac{\bar{z}}{d}\right)^{k-1} \\ C_k &= -(1+\nu)\,\mathrm{i}\left(\frac{\bar{z}}{d}\right)^k \\ D_k &= -(1+\nu)\left(\frac{\bar{z}}{d}\right)^k \qquad\qquad k = 1, 2, \ldots \end{aligned}\right\} \tag{16}$$

($\mathrm{i} = \sqrt{-1}$, $z = x + \mathrm{i}y$, $\bar{z} = x - \mathrm{i}y$, d — scaling factor equal to the average distance between the element center and the element corners) and uses them in the following generating sequence:

$$\mathbf{M}^{\mathrm{m}} = [\mathbf{M}_1^{\mathrm{m}}, \mathbf{M}_2^{\mathrm{m}}, \ldots] = E\left[\begin{array}{cccc} \mathrm{Re}\,B_1 & \mathrm{Re}\,C_1 & \mathrm{Re}\,D_1 & \vdots \\ \mathrm{Im}\,B_1 & \mathrm{Im}\,C_1 & \mathrm{Im}\,D_1 & \vdots \\ & & & \\ \mathrm{Re}\,A_2 & \mathrm{Re}\,B_2 & \mathrm{Re}\,C_2 & \mathrm{Re}\,D_2 \;\vdots \\ \mathrm{Im}\,A_2 & \mathrm{Im}\,B_2 & \mathrm{Im}\,C_2 & \mathrm{Im}\,D_2 \;\vdots \\ & & & \\ \mathrm{Re}\,A_3 & \mathrm{Re}\,B_3 & \ldots & \text{etc.} \\ \mathrm{Im}\,A_3 & \mathrm{Im}\,B_3 & \ldots & \text{etc.} \end{array}\right] \tag{17}$$

The absence of the term with A_1 in this sequence is due to the fact that $u = \mathrm{Re}\,A_1$, $v = \mathrm{Im}\,A_1$ result in a vanishing strain mode (rigid rotation).

The displacement frame

$$\tilde{\mathbf{v}}^{\,\mathrm{m}} = \left\{\begin{array}{c} \tilde{u} \\ \tilde{v} \end{array}\right\} \tag{18}$$

along a particular side $A - C - B$ of the element (Fig. 3) may be expressed in terms of the two nodal displacement vectors at corner nodes A and B,

$$\mathbf{d}_A^{\mathrm{m}} = \{\tilde{u}_A \;\; \tilde{v}_A\}^{\mathrm{T}}, \qquad \mathbf{d}_B^{\mathrm{m}} = \{\tilde{u}_B \;\; \tilde{v}_B\}^{\mathrm{T}} \tag{19a,b}$$

and of a vector containing an optional number of hierarchic side-mode DOF, attached for convenience to mid-side node C,

$$\mathbf{d}_C^{\mathrm{m}} = \left\{ {}^1\Delta\tilde{u}_C \;\; {}^1\Delta\tilde{v}_C \;\vdots\; {}^2\Delta\tilde{u}_C \;\; {}^2\Delta\tilde{v}_C \;\vdots\; \ldots \right\}^{\mathrm{T}}. \tag{19c}$$

With the frame functions displayed in Fig. 3, the components $\tilde{u}$ and $\tilde{v}$ have along the element side $A - C - B$ the following distribution:

$$\begin{aligned} \tilde{u} &= \tilde{N}_1\tilde{u}_A + \tilde{N}_2\tilde{u}_B + \tilde{N}_3\,{}^1\Delta\tilde{u}_C + \tilde{N}_5\,{}^2\Delta\tilde{u}_C + \ldots \\ &= \tilde{N}_1\tilde{u}_A + \tilde{N}_2\tilde{u}_B + \sum_{k=1,2,\ldots} \tilde{N}_{2k+1}\,{}^k\Delta\tilde{u}_C \end{aligned} \tag{20a}$$

$$\tilde{v} = \tilde{N}_1\tilde{v}_A + \tilde{N}_2\tilde{v}_B + \sum_{k=1,2,\ldots} \tilde{N}_{2k+1}\,{}^k\Delta\tilde{v}_C\,. \tag{20b}$$

The use of the above expressions, specific to plane elasticity, along with the general HT-element relations (7) and (8a–d) yields the uncoupled membrane terms $\overset{\circ}{\mathbf{r}}{}^{\mathrm{m}}$ and $\mathbf{k}^{\mathrm{m}}$ in the force–displacement relationship (9a).

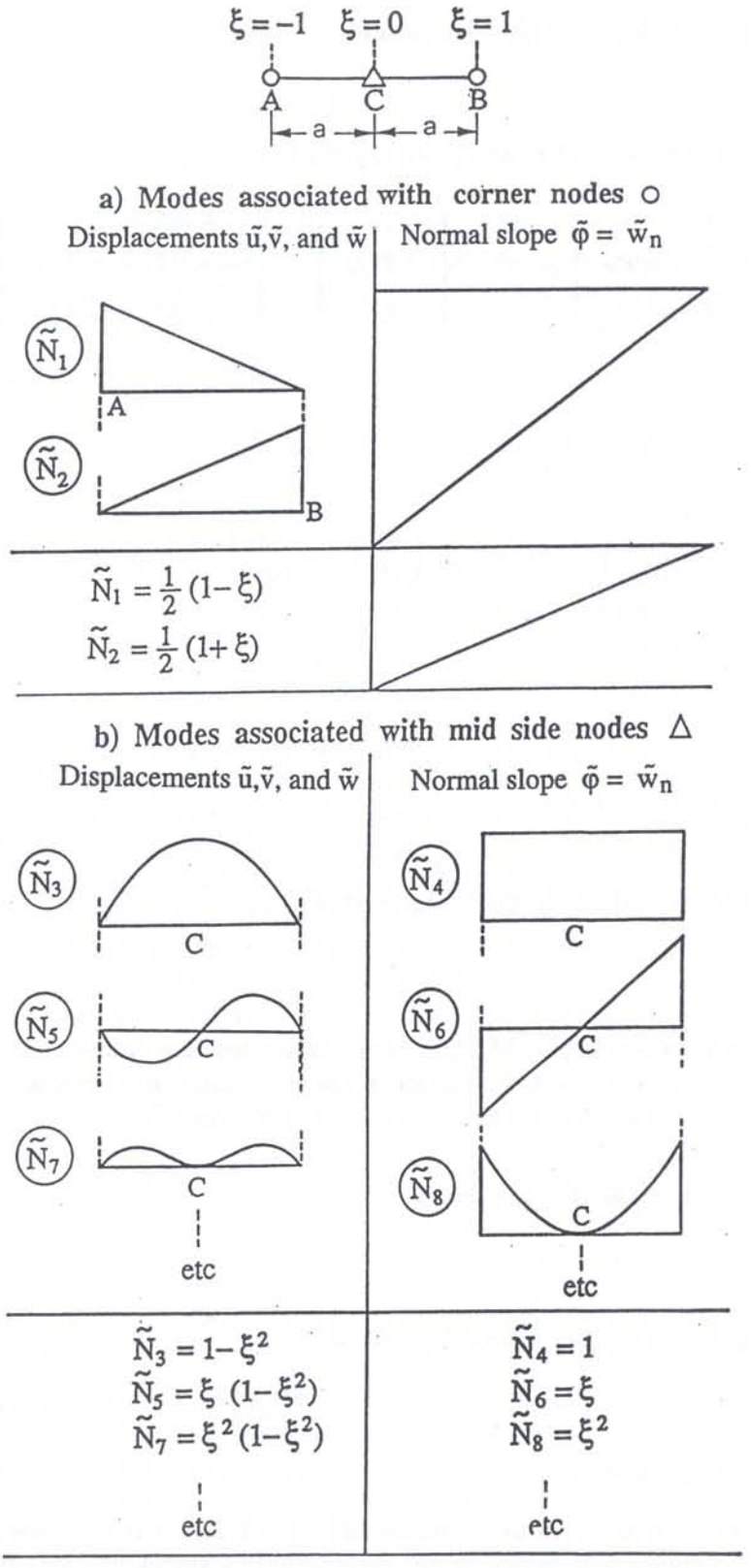

Fig. 3. Frame functions of HT folded plate *p*-element with 3 DOF at element corners and an optional number (M) of DOF at mid-side nodes

2.2.3. Plate bending component

Here the internal field $\mathbf{u}^{\mathrm{b}}$ has a single component

$$\mathbf{u}^{\mathrm{b}} = \{\mathbf{w}\} \tag{21}$$

and the conjugate vectors $\mathbf{v}^{\mathrm{b}}$ and $\mathbf{t}^{\mathrm{b}}$ at Γ^e are assumed as

$$\mathbf{v}^{\mathrm{b}} = \begin{Bmatrix} w \\ w_x \\ w_y \end{Bmatrix} = \begin{Bmatrix} w \\ \partial w/\partial x \\ \partial w/\partial y \end{Bmatrix}, \quad \mathbf{t}^{\mathrm{b}} = \begin{Bmatrix} Q_n \\ -M_{nx} \\ -M_{ny} \end{Bmatrix} = \begin{Bmatrix} n_x Q_x + n_y Q_y \\ -n_x M_x - n_y M_{xy} \\ -n_y M_y - n_x M_{xy} \end{Bmatrix}, \tag{22a,b}$$

where

$$Q_x = -D\frac{\partial}{\partial x}\nabla^2 w\,, \quad Q_y = -D\frac{\partial}{\partial y}\nabla^2 w\,, \tag{23a,b}$$

$$M_x = -D\left(\frac{\partial^2 w}{\partial x^2} + \nu\frac{\partial^2 w}{\partial y^2}\right), \quad M_y = -D\left(\frac{\partial^2 w}{\partial y^2} + \nu\frac{\partial^2 w}{\partial x^2}\right), \tag{23c,d}$$

$$M_{xy} = -D\,(1-\nu)\,\frac{\partial^2 w}{\partial x \partial y} \tag{23e}$$

and where

$$D = \frac{Et^3}{12\,(1-\nu^2)}\,. \tag{24}$$

The governing differential plate equation is stated as

$$\nabla^4 w = \frac{\bar{b}_z}{D}\,, \tag{25}$$

where $\nabla^4 = \partial^4/\partial x^4 + 2\partial^4/\partial x^2 \partial y^2 + \partial^4/\partial y^4$ and $\bar{b}_z$ stands for distributed load. The particular part of the solution may be found easily for various types of continous or discontinous loads [8]. Here, as an example, will only be given the two simplest of them, namely

$$\overset{\circ}{w} = \frac{\bar{b}_z r^4}{64D} \quad \text{for uniform load } \bar{b}_z = \text{const} \tag{26a}$$

and

$$\overset{\circ}{w} = \frac{\bar{P}_z}{16\pi D} r_P^2 \ln r_P^2 \quad \text{for concentrated load } \bar{P}_z \text{ at } x_P, y_P \tag{26b}$$

where

$$r_P^2 = (x - x_P)^2 + (y - y_P)^2\,. \tag{26c}$$

A T-complete set of homogeneous solutions M_j^{b} $(j = 1, 2, \ldots)$ is conveniently assumed in the form of biharmonic polynomials, which can be generated in a systematic way by taking in turn the real and the imaginary parts of two complex functions,

$$A_k = \left(\frac{r}{d}\right)^2 \left(\frac{z}{d}\right)^k \quad \text{and} \quad B_k = \left(\frac{z}{d}\right)^{k+2} \tag{27a,b}$$

($r^2 = x^2 + y^2$, d — scaling factor as in paragraph 2.2.2), namely:

$$\mathbf{M}^{\mathrm{b}} = \left[\mathbf{M}_1^{\mathrm{b}} \;\; \mathbf{M}_2^{\mathrm{b}}, \ldots\right] = \Big[\begin{array}{cccc} \mathrm{Re}\, A_0 & \mathrm{Re}\, B_0 & \mathrm{Im}\, B_0 & \vdots \\ \mathrm{Re}\, A_1 & \mathrm{Im}\, A_1 & \mathrm{Re}\, B_1 & \mathrm{Im}\, B_1 \quad \vdots \\ \mathrm{Re}\, A_2 & \mathrm{Im}\, A_2 & \mathrm{Re}\, B_2 & \mathrm{Im}\, B_2 \quad \vdots \quad \ldots \quad \text{etc.} \end{array} \Big] . \tag{27c}$$

As $\mathrm{Im}\,(z/d) = 0$, this generating sequence yields for $k = 0$ only three homogeneous solutions.

The components of the displacement frame vector $\tilde{\mathbf{v}}$ may conveniently be expressed in terms of two functions, $\tilde{w}$ (transverse displacement) and $\tilde{\varphi} = \tilde{w}_n$ (normal rotation), namely

$$\tilde{v} = \left\{ \begin{array}{c} \tilde{w} \\ \tilde{w}_x \\ \tilde{w}_y \end{array} \right\} = \left\{ \begin{array}{c} \tilde{w} \\ \bar{n}_x \tilde{\varphi} - \bar{n}_y \partial \tilde{w}/\partial s \\ \bar{n}_y \tilde{\varphi} + \bar{n}_x \partial \tilde{w}/\partial s \end{array} \right\}, \tag{28}$$

where

$$\partial/\partial s = -\bar{n}_y \partial/\partial x + \bar{n}_x \partial/\partial y \tag{28a}$$

and where for a particular boundary segment $A - C - B$ (Fig. 2) of length $l_{AB} = 2a$

$$\bar{n}_x = \frac{1}{l_{AB}} (y_B - y_A), \quad \bar{n}_y = -\frac{1}{l_{AB}} (x_B - x_A) . \tag{28b,c}$$

If the segment $A - C - B$ belongs to the interelement boundary, common to two neighbouring elements, then $\bar{n}_x$ and $\bar{n}_y$ are equal to the components n_x and n_y of the unit vector of the external normal of the one of the two elements along the boundary of which the sequence $A - C - B$ defines the anticlockwise rotation (Fig. 2). They are equal to $-n_x$ and $-n_y$ for the element where the sequence $A - C - B$ corresponds to the opposite sense of rotation.

In order to ensure the conformity of displacements along a common side $A - C - B$ of two or more not-coplanar elements, the transverse displacement $\tilde{w}$ will be interpolated in the same way as the in-plane displacements $\tilde{u}$ and $\tilde{v}$ in paragraph 2.2.2. On the other hand, the C^1 conformity will be enforced through the frame function $\tilde{\varphi}$, defined independently of $\tilde{w}$, only in terms of hierarchic normal rotation parameters associated with the mid-side node C. As a consequence, the subvectors of nodal parameters in A, B and C are now assumed as follows:

$$\mathbf{d}_A^{\mathrm{b}} = \{\tilde{w}_A\}, \quad \mathbf{d}_B^{\mathrm{b}} = \{\tilde{w}_B\} \tag{29a,b}$$

and

$$\mathbf{d}_C^{\mathrm{b}} = \Big\{ \begin{array}{ccccccccc} \tilde{\varphi}_C & \vdots & {}^1\Delta\tilde{w}_C & {}^1\Delta\tilde{\varphi}_C & \vdots & {}^2\Delta\tilde{w}_C & {}^2\Delta\tilde{\varphi}_C & \vdots & \ldots \quad \text{etc.} \end{array} \Big\}^{\mathrm{T}} . \tag{29c}$$

With the shape functions displayed in Fig. 3, $\tilde{w}$ and $\tilde{\varphi}$ along the element side $A - C - B$ now have the following definition:

$$\begin{aligned} \tilde{w} &= \tilde{N}_1 \tilde{w}_A + \tilde{N}_2 \tilde{w}_B + \tilde{N}_3 {}^1\Delta\tilde{w}_C + \tilde{N}_5 {}^2\Delta\tilde{w}_C + \ldots \\ &= \tilde{N}_1 \tilde{w}_A + \tilde{N}_2 \tilde{w}_B + \sum_{k=1,2,\ldots} \tilde{N}_{2k+1} {}^k\Delta\tilde{w}_C , \end{aligned} \tag{30a}$$

$$\begin{aligned} \tilde{\varphi} &= \tilde{N}_4 \tilde{\varphi}_C + \tilde{N}_6 {}^1\Delta\tilde{\varphi}_C + \tilde{N}_8 {}^2\Delta\tilde{\varphi}_C + \ldots \\ &= \tilde{N}_4 \tilde{\varphi}_C + \sum_{k=1,2,\ldots} \tilde{N}_{2k+4} {}^k\Delta\tilde{\varphi}_C . \end{aligned} \tag{30b}$$

The possibility of using in the HT Kirchhoff plate formulation an 'underconforming' displacement frame with a single parameter at element corners has for the first time been investigated and justified in Ref. [9].

As in the case of the plane elasticity component (paragraph 2.2.2), the use of general relations (7a,b) and (8a,b) along with the specific expressions of this paragraph yields the terms $\overset{\circ}{\mathbf{r}}{}^{\mathrm{b}}$ and $\mathbf{k}^{\mathrm{b}}$ in the force–displacement relationship (9b).

2.2.4. Evaluation of the resulting global force–displacement relationship of the folded plate p-element

We designate by $\mathbf{Q}$ the 3×3 transformation matrix involved in the global to local Cartesian coordinate transformation

$$\mathbf{x} = \mathbf{Q}\,(\mathbf{X} - \mathbf{X}_O)\ , \tag{31}$$

where $\mathbf{x} = \{x, y, z\}$, $\mathbf{X} = \{X, Y, Z\}$ and where $\mathbf{X}_O$ (see Fig. 2) stands for position vector of the origin O of local coordinates of the element. For future use, we split the matrix $\mathbf{Q}$ into two parts, $\mathbf{Q}^{\mathrm{m}}$ and $\mathbf{Q}^{\mathrm{b}}$ defined as

$$\mathbf{Q}^{\mathrm{m}} = \begin{bmatrix} Q_{11} & Q_{12} & Q_{13} \\ Q_{21} & Q_{22} & Q_{23} \end{bmatrix} \quad \text{and} \quad \mathbf{Q}^{\mathrm{b}} = \begin{bmatrix} Q_{31} & Q_{32} & Q_{33} \end{bmatrix}. \tag{31a,b}$$

Let now the vector of global DOF of the element in (10) be assumed as

$$\mathbf{D} = \left\{ \begin{array}{cccc} \mathbf{D}_1^{\mathrm{T}} & \mathbf{D}_2^{\mathrm{T}} & \dots & \mathbf{D}_N^{\mathrm{T}} \end{array} \right\}^{\mathrm{T}}, \tag{32}$$

where N is the number of element nodes ($N = 8$ for a quadrilateral element) and where $\mathbf{D}_i$ ($i = 1, 2, \dots N$) stand for subvectors of nodal DOF belonging alternatively to nodes ∘ at element angles (odd i) with 3 DOF,

$$\mathbf{D}_i = \left\{ \begin{array}{ccc} \tilde{U}_i & \tilde{V}_i & \tilde{W}_i \end{array} \right\}^{\mathrm{T}}, \tag{32a}$$

and to mid-side nodes △ (even i) with an optional number (M) of DOF,

$$\begin{aligned} \mathbf{D}_i = \Big\{ & \tilde{\varphi}_i \ \vdots\ {}^1\Delta\tilde{U}_i \ {}^1\Delta\tilde{V}_i \ {}^1\Delta\tilde{W}_i \ {}^1\Delta\tilde{\varphi}_i \ \vdots \\ & {}^2\Delta\tilde{U}_i \ {}^2\Delta\tilde{V}_i \ {}^2\Delta\tilde{W}_i \ {}^2\Delta\tilde{\varphi}_i \ \vdots \ \dots \Big\}^{\mathrm{T}}. \end{aligned} \tag{32b}$$

While the displacements are represented by their global Cartesian components, the rotations keep their local form ($\tilde{\varphi} = \tilde{w}_n$ where $\tilde{w}$ is the out-of-plane displacement), as they do in the vectors $\mathbf{d}^{\mathrm{m}}$ and $\mathbf{d}^{\mathrm{b}}$ of local DOF of paragraphs 2.2.2 and 2.2.3.

Instead of forming explicitly the transformation matrix $\mathbf{L}$ in (10c) for the whole element, it is computationally more efficient to perform the transformations node by node. Thus for each i the vectors $\overset{\circ}{\mathbf{r}}{}_i^{\mathrm{m}}$ and $\overset{\circ}{\mathbf{r}}{}_i^{\mathrm{b}}$ are converted into $\overset{\circ}{\mathbf{R}}_i$ and for each i and $j \geq i$ (to account for the symmetry),the matrices $\mathbf{k}_{ij}^{\mathrm{m}}$ and $\mathbf{k}_{ij}^{\mathrm{b}}$ are converted into $\mathbf{K}_{ij}$. Provided that all mid-side nodes of the element have the same number (M) of DOF, only 4 smaller transformation matrices need to be evaluated:

- matrices $\mathbf{L}_A^{\mathrm{m}}$ (2×3) and $\mathbf{L}_A^{\mathrm{b}}$ (1×3) common to all element corner nodes ∘,
- matrices $\mathbf{L}_C^{\mathrm{m}}$ $(M^{\mathrm{m}} \times M)$ and $\mathbf{L}_C^{\mathrm{b}}$ $(M^{\mathrm{b}} \times M)$ common to all mid-side nodes △.

Table 1. Optional numbers M of global DOF at mid-side nodes and corresponding numbers of local DOF for membrane(M^m) and plate bending (M^b) components

M	1	5	9	13	17	etc.
M^{m}	0	2	4	6	8	etc.
M^{b}	1	3	5	7	9	etc.

Note that M^{m} and M^{b} in the above (Table 1) stand for the numbers of membrane and plate bending DOF which correspond in the local reference frame to the optional number M of global DOF at the mid-side nodes of the element. These matrices transform the subvectors of the global DOF $\mathbf{D}_i$ at corner nodes $\circ$ or mid-side nodes $\triangle$ into the subvectors of the local DOF $\mathbf{d}_i^{\mathrm{m}}$ and $\mathbf{d}_i^{\mathrm{b}}$, namely

$$\mathbf{d}_i^{\mathrm{m}} = \mathbf{L}_A^{\mathrm{m}}\mathbf{D}_i \quad \text{and} \quad \mathbf{d}_i^{\mathrm{b}} = \mathbf{L}_A^{\mathrm{b}}\mathbf{D}_i \quad \text{at element angles,} \tag{33a,b}$$

$$\mathbf{d}_i^{\mathrm{m}} = \mathbf{L}_C^{\mathrm{m}}\mathbf{D}_i \quad \text{and} \quad \mathbf{d}_i^{\mathrm{b}} = \mathbf{L}_C^{\mathrm{b}}\mathbf{D}_i \quad \text{at mid-side nodes.} \tag{33c,d}$$

Observing that in (33a,b), respectively (33c,d), the definitions of $\mathbf{d}_i^{\mathrm{m}}$ and $\mathbf{d}_i^{\mathrm{b}}$ are identical to those obtained through the replacement of A by i, respectively C by i in (19a) and (19c), respectively (29a) and (29c), makes it possible to obtain explicitly the following transformation matrices:

- nodes $\circ$ (odd i)

$$\mathbf{L}_A^{\mathrm{m}} = \mathbf{Q}^{\mathrm{m}} \quad \text{and} \quad \mathbf{L}_A^{\mathrm{b}} = \mathbf{Q}^{\mathrm{b}}, \tag{34a,b}$$

- nodes $\triangle$ (even i, assumed $M = 9$)

$$\mathbf{L}_C^{\mathrm{m}} = \begin{bmatrix} \mathbf{0}_{21} & \vdots & \mathbf{Q}^{\mathrm{m}} & \mathbf{0}_{21} & \vdots & \mathbf{0}_{23} & \mathbf{0}_{21} \\ \cdots & \cdots & \cdots & \cdots & \cdots & \cdots & \cdots \\ \mathbf{0}_{21} & \vdots & \mathbf{0}_{23} & \mathbf{0}_{21} & \vdots & \mathbf{Q}^{\mathrm{m}} & \mathbf{0}_{21} \end{bmatrix}, \tag{34c}$$

$$\mathbf{L}_C^{b} = \begin{bmatrix} 1 & \vdots & \mathbf{0}_{13} & 0 & \vdots & \mathbf{0}_{13} & 0 \\ \cdots & \cdots & \cdots & \cdots & \cdots & \cdots & \cdots \\ 0 & \vdots & \mathbf{Q}^{\mathrm{b}} & 0 & \vdots & \mathbf{0}_{13} & 0 \\ 0 & \vdots & \mathbf{0}_{13} & 1 & \vdots & \mathbf{0}_{13} & 0 \\ \cdots & \cdots & \cdots & \cdots & \cdots & \cdots & \cdots \\ 0 & \vdots & \mathbf{0}_{13} & 0 & \vdots & \mathbf{Q}^{\mathrm{b}} & 0 \\ 0 & \vdots & \mathbf{0}_{13} & 0 & \vdots & \mathbf{0}_{13} & 1 \end{bmatrix}, \tag{34d}$$

where $\mathbf{0}_{mn}$ stands for a $m \times n$ matrix of zeros.

With the above matrices, we may now set simply

$$\overset{\circ}{\mathbf{R}}_i = (\mathbf{L}_i^{\mathrm{m}})^{\mathrm{T}} \overset{\circ}{\mathbf{r}}{}_i^{\mathrm{m}} + \left(\mathbf{L}_i^{\mathrm{b}}\right)^{\mathrm{T}} \overset{\circ}{\mathbf{r}}{}_i^{\mathrm{b}}, \tag{35a}$$

$$\mathbf{K}_{ij} = (\mathbf{L}_i^{\mathrm{m}})^{\mathrm{T}} \mathbf{k}_{ij}^{\mathrm{m}} \mathbf{L}_j^{\mathrm{m}} + \left(\mathbf{L}_i^{\mathrm{b}}\right)^{\mathrm{T}} \mathbf{k}_{\mathrm{ij}}^{\mathrm{b}} \mathbf{L}_{\mathrm{j}}^{\mathrm{b}} \tag{35b}$$

and substitute:

$$\left.\begin{array}{llll} \mathbf{L}_i^{\mathrm{m}} = \mathbf{L}_A^{\mathrm{m}} & \text{and} & \mathbf{L}_i^{\mathrm{b}} = \mathbf{L}_A^{\mathrm{b}} & \text{if } i \text{ is odd} \\ \mathbf{L}_i^{\mathrm{m}} = \mathbf{L}_C^{\mathrm{m}} & \text{and} & \mathbf{L}_i^{\mathrm{b}} = \mathbf{L}_C^{\mathrm{b}} & \text{if } i \text{ is even} \\ \mathbf{L}_j^{\mathrm{m}} = \mathbf{L}_A^{\mathrm{m}} & \text{and} & \mathbf{L}_j^{\mathrm{b}} = \mathbf{L}_A^{\mathrm{b}} & \text{if } j \text{ is odd} \\ \mathbf{L}_j^{\mathrm{m}} = \mathbf{L}_C^{\mathrm{m}} & \text{and} & \mathbf{L}_j^{\mathrm{b}} = \mathbf{L}_C^{\mathrm{b}} & \text{if } j \text{ is even} \end{array}\right\}. \tag{35c–f}$$

2.2.5. Implementation

Since no area integration is needed, a single FE subroutine may cover a family of folded plate p-elements presenting a polygonal boundary (Fig. 2) with an optional number of sides. Such a subroutine should automatically adjust the number m of homogeneous T-functions of the internal displacement field of the element to its number of sides and the optional number of side-mode DOF of each of them.

The rank condition of a HT p-element states that [1] a minimum of

$$m = \mathrm{NDOF} - \mathrm{NRIG} \tag{36}$$

linearly independent T-functions (NDOF — number of nodal DOF, NRIG — number of rigid body modes) is necessary, but sometimes not sufficient, for its stiffness matrix to have full rank. In our case such a rule should separately hold for each of the two uncoupled folded plate components — the membrane component (9a) and the plate bending component (9b) — later combined into a single force–displacement relationship (9c). If attention is focused on the quadrilateral element — only this member of the element family was used in the numerical studies of Section 3 — then the minimum of

$$m^{\mathrm{m}} = 4M^{\mathrm{m}} + 5 \quad \text{respectively} \quad m^{\mathrm{b}} = 4M^{\mathrm{b}} + 1 \tag{37a,b}$$

linearly independent T-functions, have to be used to evaluate the stiffness matrix $\mathbf{k}^{\mathrm{m}}$, respectively $\mathbf{k}^{\mathrm{b}}$. The standard eigenvalue tests of these matrices (see [6] and [9]) have reported a vanishing number of spurious zero energy modes, thus confirming that the values of m^{m} and m^{m} shown above need not be augmented.

3. Assessment

The crucial problem of the investigated approach is its capability of reliably predicting the in-plane shear stress components in corners formed by the intersection of three or more not-coplanar panels. This problem is studied in Example 1. The remaining examples further assess the advocated approach through comparison with results available in the working literature.

3.1. Example 1 (Fig. 4)

The stiffened steel panel (Fig. 4) was subjected to uniformly distributed shear load p and solved for the following three combinations of thicknesses specified for the panels 1 to 3:

$$\left.\begin{array}{ll} 1: & t_1 = 0.01L,\ t_2 = t_3 = 0.0001L \\ 2: & t_1 = t_2 = t_3 = 0.01L \\ 3: & t_1 = 0.0001L,\ t_2 = t_3 = 0.01L \end{array}\right\}. \tag{38a–c}$$

In order to take into account the symmetry with respect to the plan ($Z = 0$), only the part $Z \geq 0$ of the structure was considered while imposing $\tilde{W} = 0$ for $Z = 0$. The calculation for each of the above combinations of thicknesses was performed for the following discretizations:

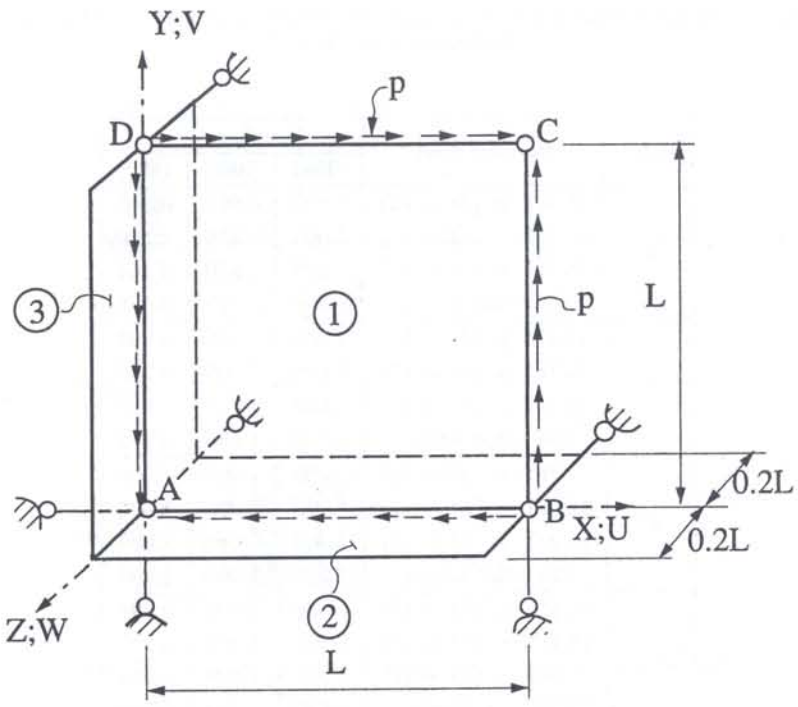

Fig. 4. Example 1: Stiffened steel panel ($\nu = 0.3$, $L = 1000$ mm) under uniform shear load

- Mesh of 15 HT folded plate elements (3×3 elements for panel 1, 1×3 elements for panels 2 and 3) with $M = 13$, 17 and 21 side mode DOF at mid-side nodes, corresponding to a total of $N_{\mathrm{ACT}} = 363$, 463 and 563 active DOF.

- Uniform meshes of cubic isoparametric shell elements with 6 global DOF (3 displacements, 3 rotations) at nodes situated along $A - B$, $A - D$ and $A - F$ and with 5 DOF (3 global displacements, 2 local rotations) elsewere:

  Mesh 1: 2×2 elements for panel 1, 1×2 elements for panels 2 and 3; $N_{\mathrm{ACT}} = 194$ DOF

  Mesh 2: 4×4 elements for panel 1, 2×4 elements for panels 2 and 3; $N_{\mathrm{ACT}} = 686$ DOF

  Mesh 3: 8×8 elements for panel 1, 4×8 elements for panels 2 and 3; $N_{\mathrm{ACT}} = 2456$ DOF

The results displayed on Table 2 show that, although based on the Kirchhoff assumptions, the HT folded plate elements have the capability to predict reasonably well, for a large range of ratios of thicknesses, the in-plane shear force at the corner formed by the intersection of the three not-coplanar panels. While the first (38a) and the third (38c) combinations of thicknesses produce, at point A in panel 1, results close to those tending at the limit respectively to $N_{XY} = p$ (pure shear) and $N_{XY} = 0$, the combination (38b) is an intermediate case. Note also that the HT element results seem to converge to those predicted by the solution with a mesh of 128 cubic isoparametric shell elements, based on the Reissner–Mindlin assumption and integrated numerically with $3 \times 3 \times 2$ Gauss points. In spite of a very large number of unknowns, this reference solution is, unfortunately, not yet fully converged (see e.g. the predicted shear force at the free corner of panel 1, in the last column of Table 2).

The study is completed by a comparison of results for displacements at corner points (Table 3) and distribution of shear forces N_{XY} in the panel 1 along its diagonal $A - C$ (Figs. 5 to 7). These results clearly show the purely local character of the steep gradient solution in the neighbourhood of the corner A, which cannot be accurately represented without a local refinement of the FE mesh, but which has only little influence on the solution elsewhere.

Table 2. Example 1: In-plane shear force $N_{XY} : p$ at corners of panel 1 (Fig. 2) for three combinations of thicknesses (see (38a–c))

Point	Element mesh	Case		
		(38a)	(38b)	(38c)
A	15 HT–p, $(M = 13)$	1.000	0.961	0.313
	15 HT–p, $(M = 17)$	1.000	0.926	0.230
	15 HT–p, $(M = 21)$	1.000	0.870	0.164
	128 cubic isopar.	1.000	0.819	0.078
B	15 HT–p, $(M = 13)$	1.000	1.000	0.999
	15 HT–p, $(M = 17)$	1.000	1.000	0.999
	15 HT–p, $(M = 21)$	1.000	1.000	0.999
	128 cubic isopar.	1.000	1.000	0.999
C	15 HT–p, $(M = 13)$	1.000	1.000	1.000
	15 HT–p, $(M = 17)$	1.000	1.000	1.000
	15 HT–p, $(M = 21)$	1.000	1.000	1.000
	128 cubic isopar.	1.000	1.000	1.000
D	15 HT–p, $(M = 13)$	1.000	1.000	0.999
	15 HT–p, $(M = 17)$	1.000	1.000	0.999
	15 HT–p, $(M = 21)$	1.000	1.000	0.999
	128 cubic isopar.	1.000	1.000	0.996

Table 3. Example 1: Global displacement components $EU : p$ and $EV : p$ at corner points

Point	Quantity	Element mesh	Case		
			(38a) $10^2\times$	(38b) $10^2\times$	(38c) $10^4\times$
B	$EU : p$	15 HT–p, $(M = 13)$	–0.000	–0.000	–0.000
		15 HT–p, $(M = 17)$	0.000	–0.000	–0.000
		15 HT–p, $(M = 21)$	–0.000	–0.000	–0.001
		128 cubic isopar.	–0.005	–0.002	–0.001
C	$EU : p$	15 HT–p, $(M = 13)$	2.600	2.599	2.583
		15 HT–p, $(M = 17)$	2.600	2.600	2.583
		15 HT–p, $(M = 21)$	2.600	2.599	2.583
		128 cubic isopar.	2.600	2.598	2.584
	$EV : p$	15 HT–p, $(M = 13)$	0.000	–0.000	–0.010
		15 HT–p, $(M = 17)$	0.000	–0.000	–0.010
		15 HT–p, $(M = 21)$	–0.000	–0.000	–0.010
		128 cubic isopar.	–0.000	–0.000	–0.012
D	$EU : p$	15 HT–p, $(M = 13)$	2.600	2.599	2.593
		15 HT–p, $(M = 17)$	2.600	2.600	2.593
		15 HT–p, $(M = 21)$	2.600	2.600	2.593
		128 cubic isopar.	2.600	2.598	2.594
	$EV : p$	15 HT–p, $(M = 13)$	–0.000	–0.000	–0.000
		15 HT–p, $(M = 17)$	–0.000	–0.000	–0.000
		15 HT–p, $(M = 21)$	–0.000	–0.000	–0.001
		128 cubic isopar.	–0.000	–0.002	–0.001

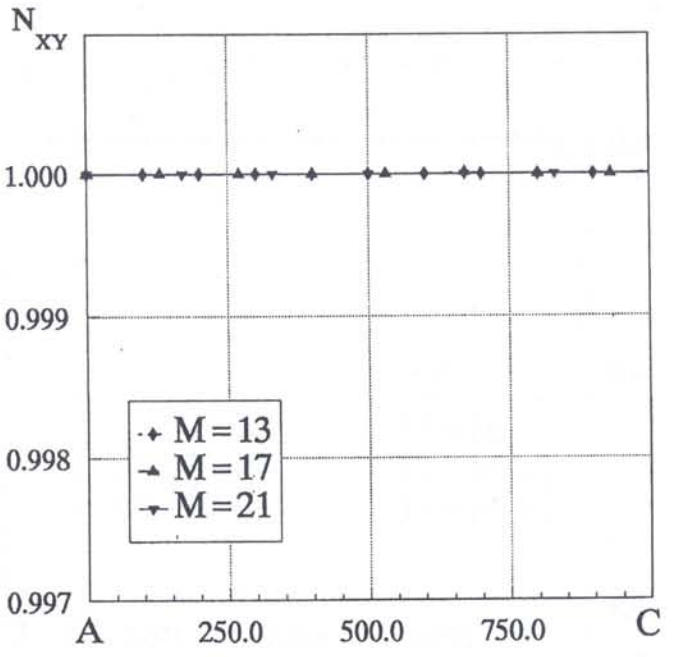

a)

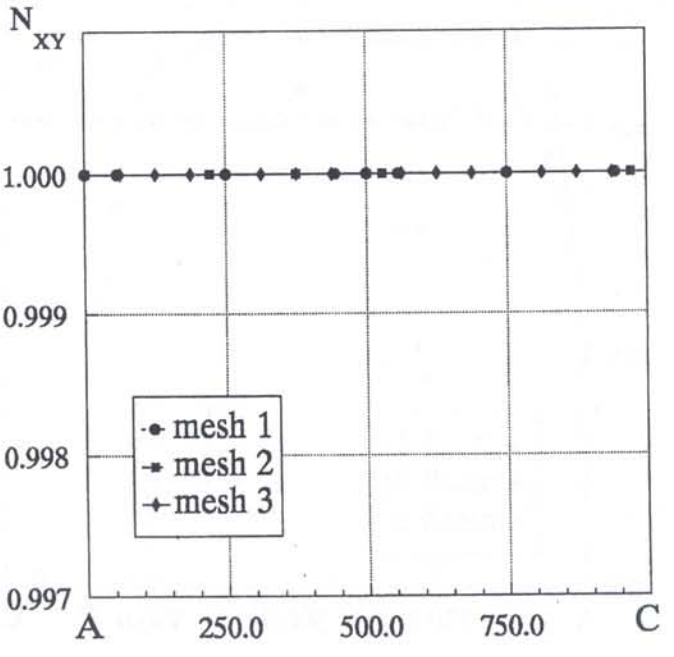

b)

Fig. 5. Example 1: Distribution along $A - C$ of shear force N_{XY} in panel 1 in case of very weak stiffeners (see (38a)). a) Uniform mesh of HT elements b) Uniform mesh of cubic isoparametric elements

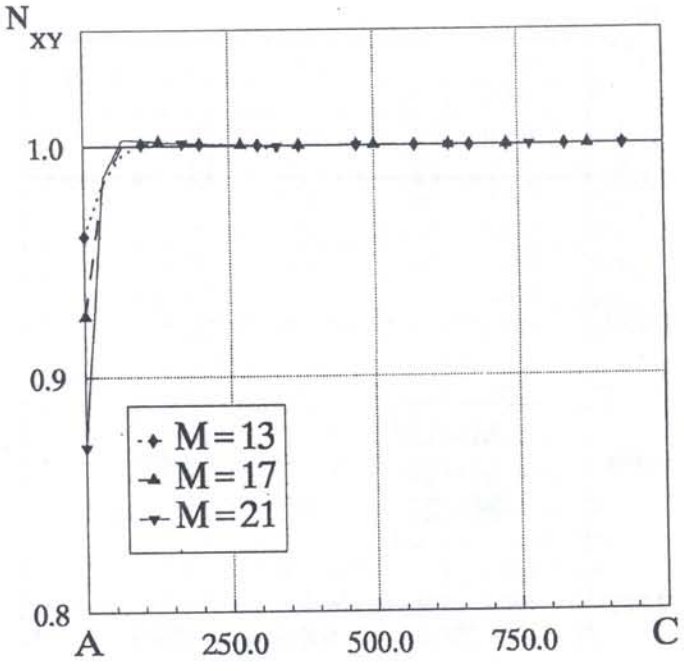

a)

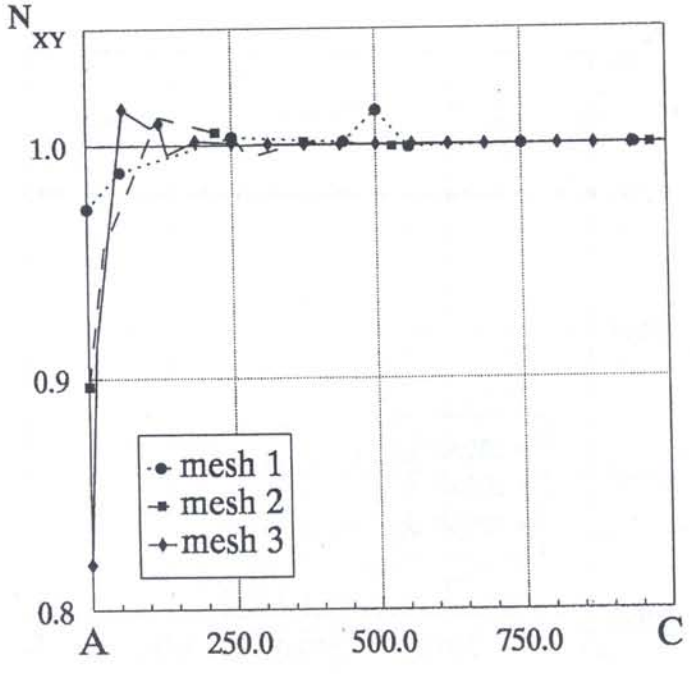

b)

Fig. 6. Example 1: Distribution along $A-C$ of shear force N_{XY} in panel 1 in case of equal thicknesses of all panels (see (38b)). a) Uniform mesh of HT elements b) Uniform mesh of cubic isoparametric elements

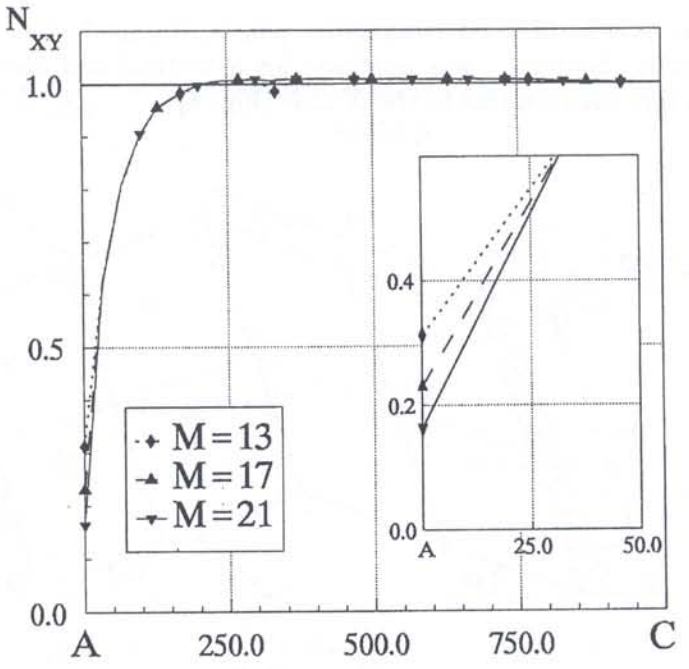

a)

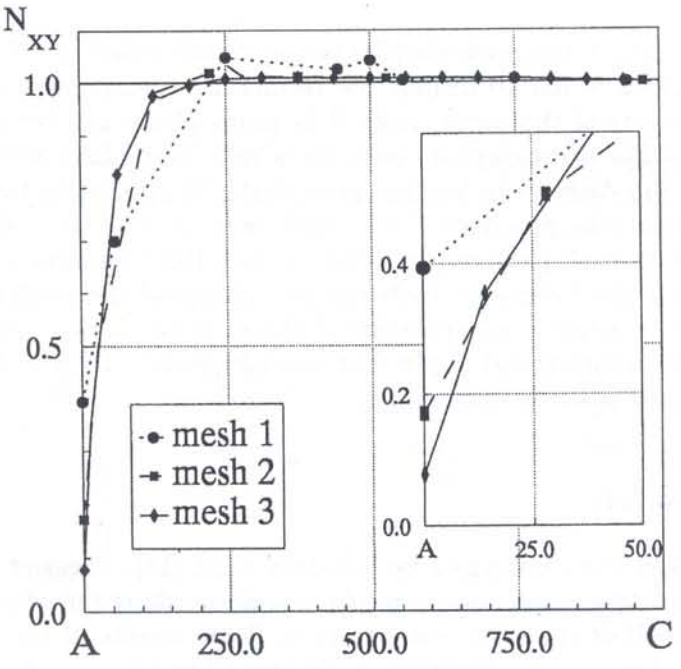

b)

Fig. 7. Example 1: Distribution along $A - C$ of shear force N_{XY} in case of very weak vertical panel (38c). a) Uniform mesh of HT elements b) Uniform mesh of cubic isoparametric elements

3.2. Example 2 (Fig. 8)

The structure formed by two inclined rectangular panels, clamped along one edge and free on the remaining part of its boundary, was analyzed for a vertical and horizontal load, uniformly distributed along the free edge parallel to the X axis (Fig. 8).

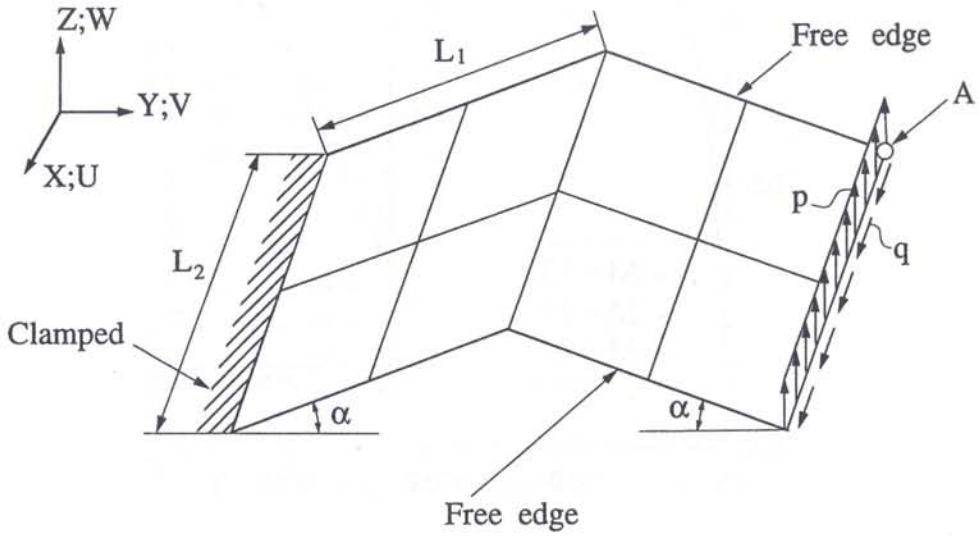

Fig. 8. Example 2: Steel structure ($\nu = 0.3$) formed by two inclined panels. $L_1 = 125$ mm, $L_2 = 100$ mm, $t = 12$ mm, $\alpha = 30°$

The HT element solution was performed for two uniform meshes, 1×2 and 3×6, with $M = 5$, 9, 13, 17 and 21. Figures 9 and 10 display the results of a convergence study of the horizontal and vertical displacements of the corner node A in terms of the number N_{ACT} of active DOF of the element assembly. The displacement components were normalized with respect to the 'exact' solution obtained by the Aitken acceleration procedure [10] applied to the three consecutive HT element solutions obtained on a uniform 7×14 mesh with $M = 13$, 17 and 21.

Figures 9 and 10 also display the results obtained with three uniform 3×6, 6×12 and 12×24 meshes of quadrilateral shell elements from the FE library of the program ANSYS [11]. These 20 DOF elements use a bilinear interpolation of the in-plane displacement components for the membrane part of the solution and apply four overlaid Batoz [12] and Razzaque [13] triangles (DKT) to represent their plate bending action.

3.3. Example 3 (Fig. 11)

This example was taken from the paper by Scordelis *et al.* [14]. The end diaphragms supporting the roof were assumed to exhibit infinite in-plane and vanishing out-of-plane rigidity. Owing to symmetry, only one half of the span was analyzed. Some results of the solution obtained with different folded plate elements are displayed on Figures 12 to 14.

The HT element solution was performed with 1×5 (single element per panel) and 3×6 (Fig. 11) meshes, each of them used in turn with $M = 5$, 9, 13, 17 and 21 DOF at mid-side nodes. It is worth mentioning that with the 3×6 mesh, excellent accuracy is observed already with 9 DOF at mid-side nodes. Further increase of the number of these DOF does not noticeably change the results. The results obtained with 3×6, 6×12 and 12×24 ANSYS folded plate elements as well as with the same meshes of the SQ2 quadrilateral shell elements [15], as displayed on Fig. 12 and 13, obviously tend to converge to the same solutions as the HT p-elements. On the other hand, the results of the analytical solution taken from Scordelis *et al.* [14], which have been obtained with

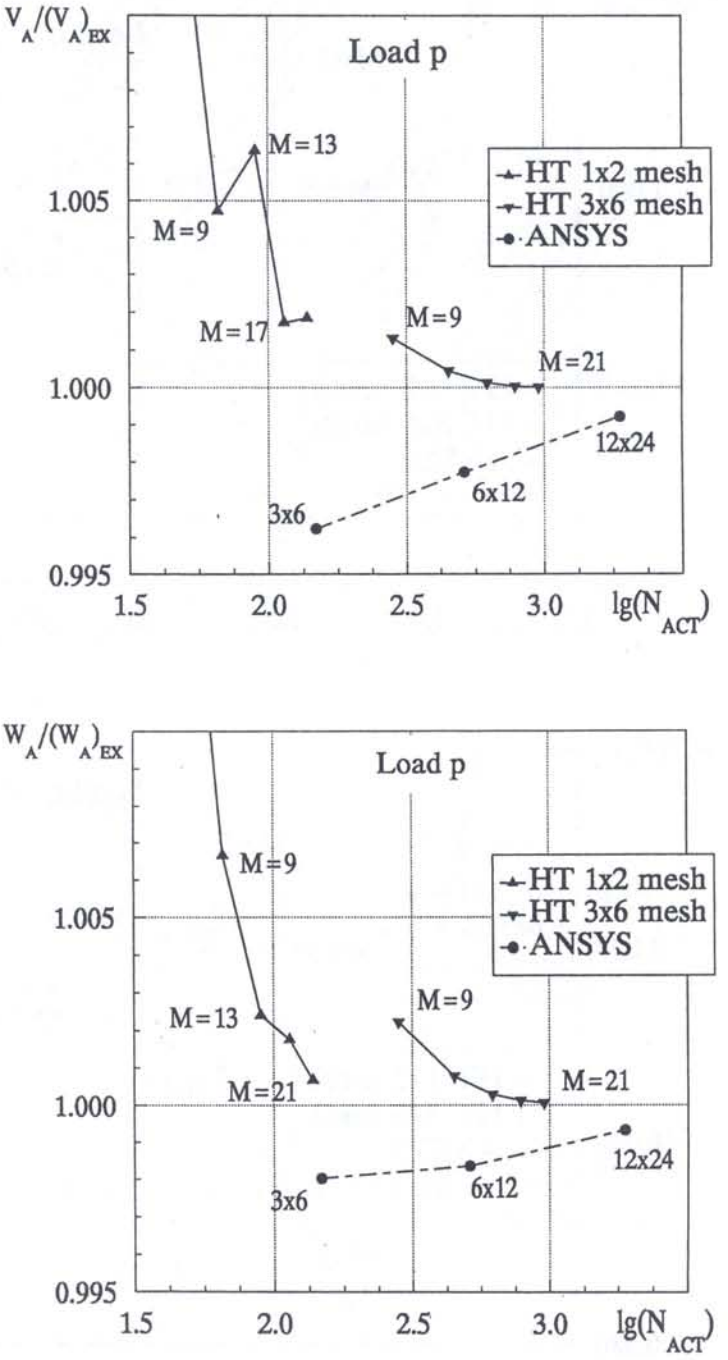

Fig. 9. Example 2: Convergence study of deflection components at corner A (Fig. 8) under vertical load p. HT-elements (M =5, 9, 13, 17, 21) and ANSYS elements (3×6, 6×12 and 12×24 meshes)

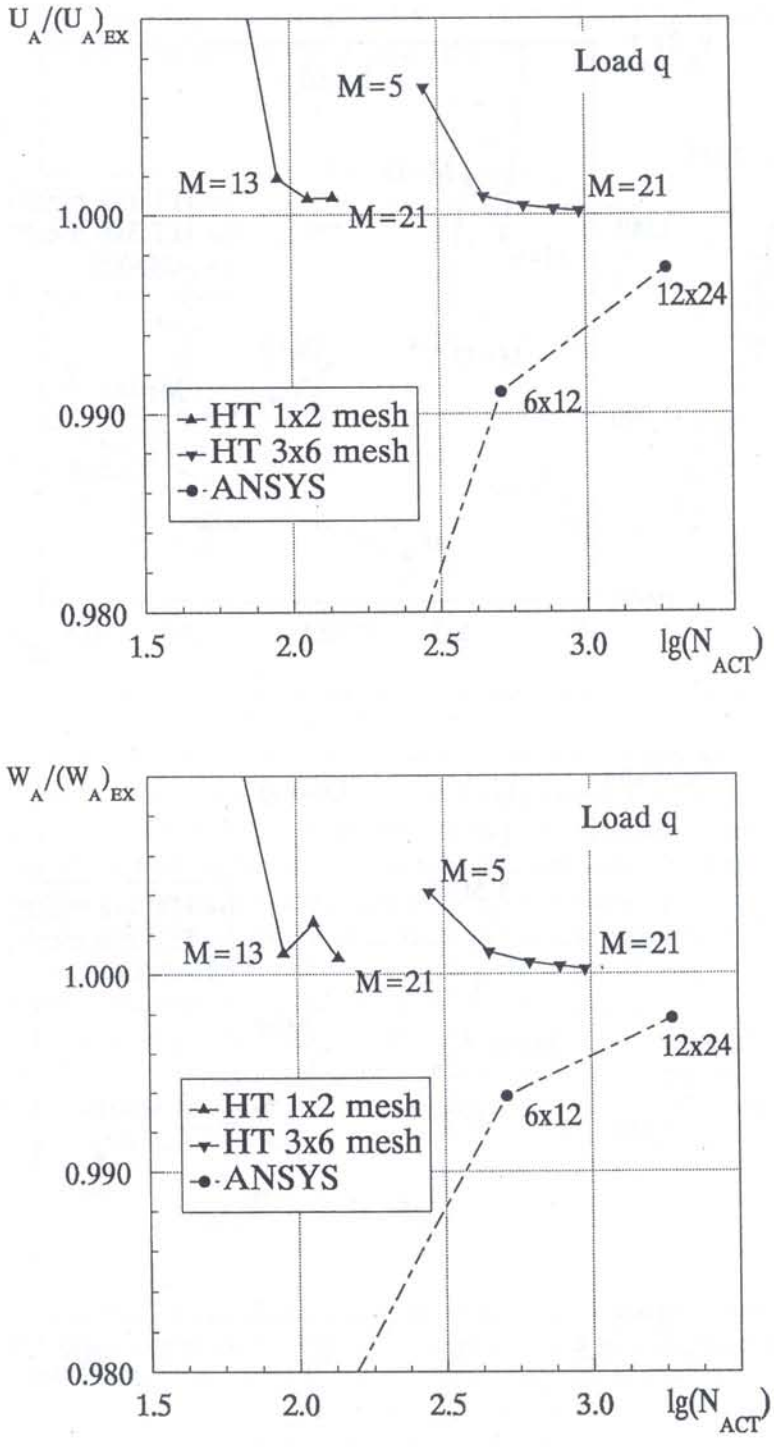

Fig. 10. Example 2: Convergence study of deflection components at corner A (Fig. 8) under horizontal load q. HT-elements (M =5, 9, 13, 17, 21) and ANSYS elements (3 × 6, 6 × 12 and 12 × 24 meshes)

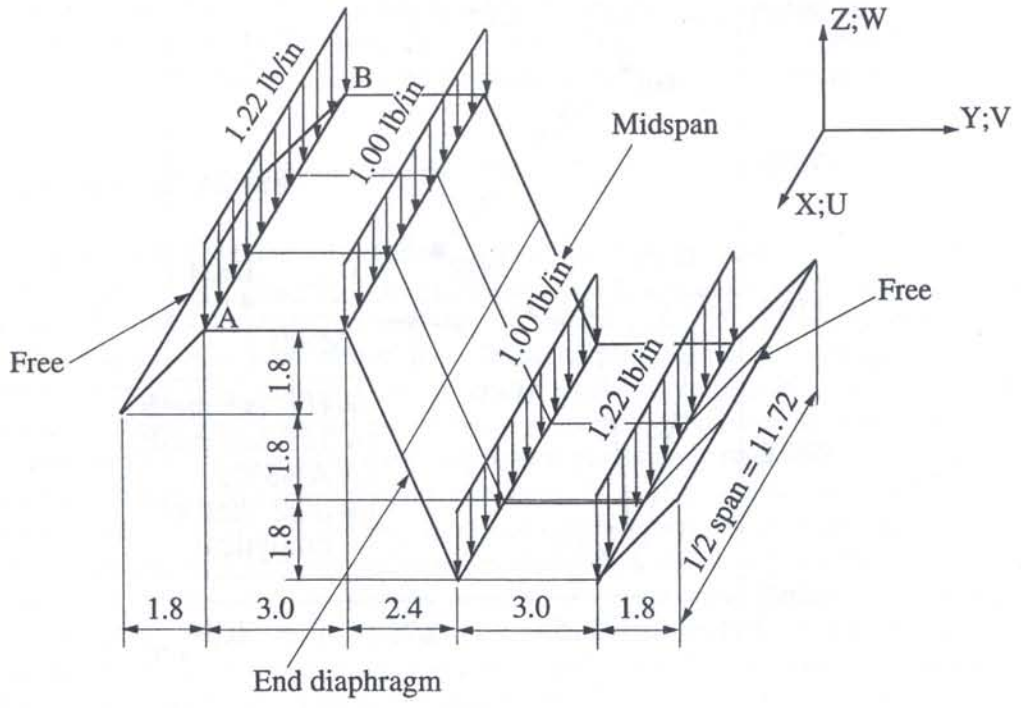

Fig. 11. Example 3: Folded plate structure with 3×6 HT element mesh. $E = 1.06 \times 10^7$ psi, $\nu = 0.3$, $t = 0.063$ in.

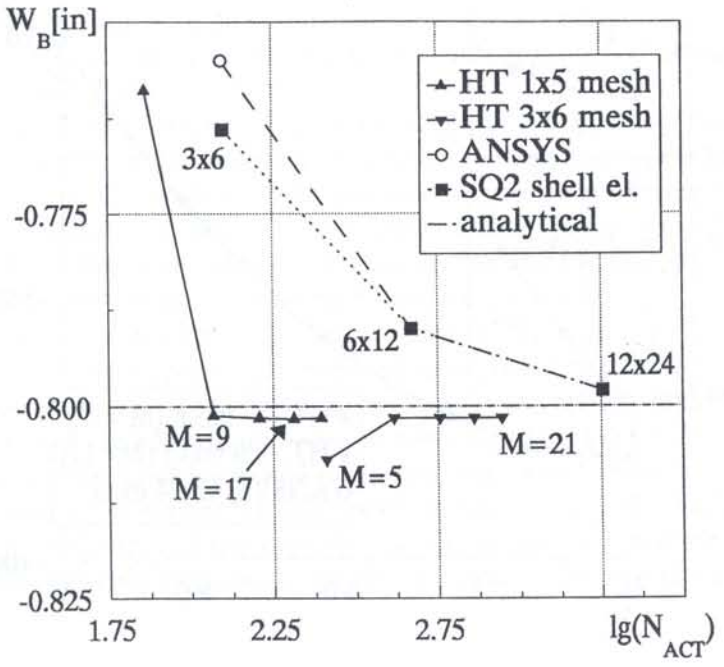

Fig. 12. Example 3: Convergence study of vertical displacement at point B (Fig. 11)

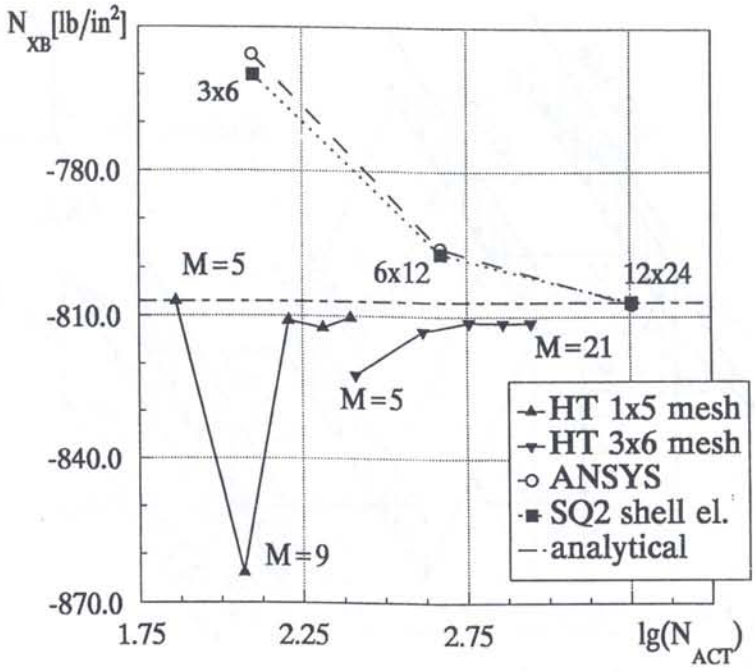

Fig. 13. Example 3: Convergence study of longitudinal membrane stress at point B (Fig. 11)

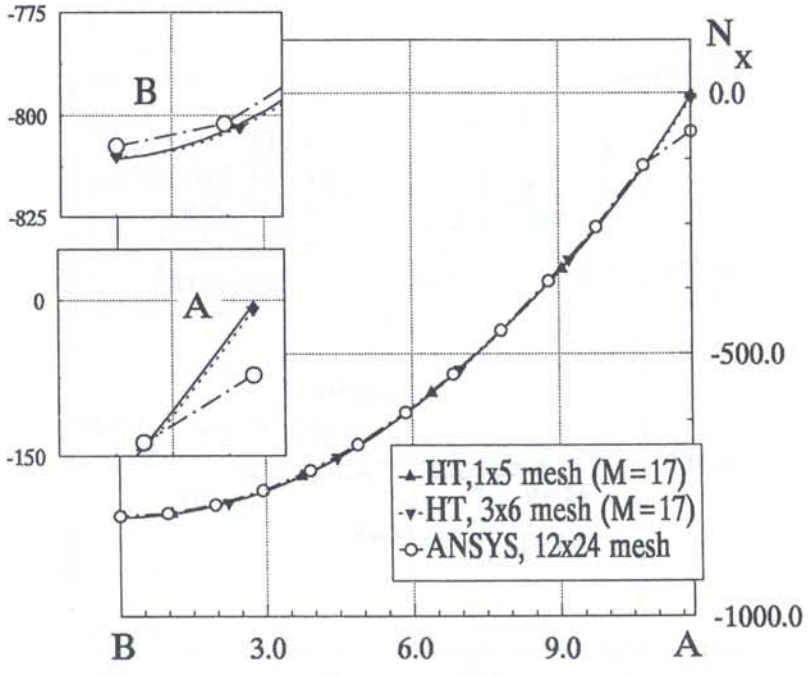

Fig. 14. Example 3: Distribution of longitudinal membrane stress along $B - A$ (Fig. 11)

only four Fourier's series terms, are not yet sufficiently converged (see the intermediate results in [14]) and cannot be used as the reference solution.

In Fig. 14, which shows the longitudinal membrane stress along the segment $B - A$, the only difference between the simplest possible HT p-element mesh (each panel represented by a single

element) and the very dense 12×24 mesh of ANSYS elements appears at the supported boundary, where the longitudinal membrane stress should vanish ($\sigma_{XA} = 0$). The error of the ANSYS element solution is here, locally, about 10 times larger than the one of the HT element solution.

4. Concluding remarks

The folded plate HT p-elements presented in this paper were obtained by coupling in a single force–displacement relationship the independent in- and out-of-plane contributions represented respectively by the plane elasticity [6] and the Kirchhoff plate [9] HT p-elements. The principal difficulty of using the Kirchhoff rather then Reissner–Mindlin plate bending theory was the C^1 conformity conditions to be enforced on the out-of-plane displacement w along the common part of the boundary of two not-coplanar panels, while permitting the in-plane shear deformation in the corner formed by three or more generally disposed non-coplanar panels. This last feature, natural in the Reissner–Mindlin type plate bending concept, is in the case of the Kirchhoff assumptions only possible if use is made of a suitably modified displacement frame formulation within the HT p-element concept. In the formulation studied in this paper, the strong requirement of conservation of the angles in the common corner of three or more not-coplanar elements was released in order to allow for the in-plane corner shear. The simplest practical approach to reaching this aim consisted in replacing the customary 'exactly and minimally conforming' displacement frame [16] by an 'underconforming' one, with only 3 DOF (displacements $\tilde{U}$, $\tilde{V}$, $\tilde{W}$) at the element corners while the normal rotation $\tilde{\varphi}$ was interpolated, independently of displacements, only in terms of the mid-side node rotation parameters. As a consequence, the definition of the out-of-plane displacement component $\tilde{w}$ was the same as that used for the in-plane components $\tilde{u}$ and $\tilde{v}$. However, the definition of the local rotation components as obtained at the element corners either from the frame function $\tilde{\varphi}$ or derived from $\tilde{w}$ was no longer unique. As was shown in [9], the admissibility of such a frame is due to the fact that the matching process between w, w_x, w_y and $\tilde{w}$, $\tilde{w}_x$, $\tilde{w}_y$ indirectly tends to enforce the missing unicity condition on the frame field since no such default exists for the assumed internal displacement field w of the element.

The new folded plate p-elements were implemented in the FE library of the general purpose FE program SAFE [17] and thoroughly assessed on a series of benchmark problems. These numerical studies, of which only a part was selected for publication, have shown that the in-plane shear at corners where three or more arbitrarily disposed not-coplanar elements meet is reliably predicted over a large range ratios of the element thicknesses. Moreover, the solution accuracy and convergence rate have favorably compared with the existing folded plate elements.

Though excellent HT plate bending p-elements based on the Reissner–Mindlin assumptions are now also available [18], the main practical interest of using the Kirchhoff plate theory in the folded plate element formulation is the simplicity of input data for specification of various boundary conditions, the lower cost of evaluation of the element matrices (the T-complete set of internal functions in [18] includes the modified Bessel functions, expensive to generate), and the availability of load terms accurately representing various patch or line loads [19]. This last facility makes it possible to accurately evaluate e.g. the moment concentrations in a box-girder bridge under the wheels of a lorry, without mesh refinement, simply as a part of the overall analysis of the bridge.

References

[1] J. Jirousek. Basis for development of large finite elements locally satisfying all field equations. *Comp. Meth. Appl. Mech. Eng.*, **14**: 65–92, 1978.

[2] J. Jirousek, A. Wróblewski. T–elements: A finite element approach with advantages of boundary solution methods. *Advances of Engng. Software*, **24**: 71–88, 1995.

[3] J. Jirousek, A. Wróblewski. T–elements: State of the art and future trends. *Archives of Comp. Meth. in Engng*, **3**: 323–434, 1996.

[4] E. Trefftz. Ein Gegenstück zum Ritzschen Verfahren. In: *Proceedings 2nd International Congress of Applied Mechanics*, 131–137, Zurich, 1926.

[5] J. Jirousek, A. Venkatesh, A. P. Zieliński, H. Rabemantantsoa, 'Comparative study of p–extensions based on conventional assumed displacement and hybrid–Trefftz FE models. *Comp. Struct.*, **46**: 261–278, 1993.

[6] J. Jirousek, A. Venkatesh. Hybrid–Trefftz plane elasticity elements with p–method capabilities. *Int. J. Numer. Meth. Eng.*, **35**: 1443–1472, 1992.

[7] J. Jirousek. Hybrid–Trefftz plate bending elements with p–method capabilities. *Int. J. Numer. Meth. Eng.*, **24**: 1367–1393, 1987.

[8] A. Venkatesh, J. Jirousek. Finite element formulation for the analysis of local effects. In: V. Krupka, M. Drdacky, eds., *Contact Loading and Local Effects in Thin Walled Plated and Shell Structures* , Berlin, Springer–Verlag, 1991.

[9] J. Jirousek, A. Wróblewski, B. Szybiński. *Alternative displacement frame formulations in hybrid–Trefftz Kirchhoff plate p–elements*. Int. Rep. LSC 96/02, Swiss Federal Institute of Technology, Lausanne, 1995, see also in present issue of CAMES.

[10] A. Aitken. On Bernoulli's numerical solution of algebraic equations. *Proc. Roy. Soc. Edinburgh*, **46**: 283–305, 1926.

[11] G. DeSalvo, R. Gorman, *ANSYS — User Manual.* Swanson Analysis System Inc., 1989.

[12] J. Batoz, K. Bathe, L. Ho. A study of three node triangular plate bending element. *Int. J. Numer. Meth. Eng.*, **15**: 1771–1812, 1980.

[13] A. Razzaque. On the four noded discrete Kirchhoff shell elements. In: J. Robinson, ed., *Accuracy Reliability Training in FEM Technology*, 473–483, 1984.

[14] A. Scordelis, E. Croy, I. Stubbs. Experimental and analytical study of a folded plate. *J. of Struct. Div. ASCE*, **87**: 139–160, 1961.

[15] A. Ibrahimbergović, F. Frey, B. Rebora. *Unified approach of modelling of complex structural systems: finite elements with rotational degrees of freedom.* Int. Rep. LSC 93/09, Swiss Federal Institute of Technology, Lausanne, 1993.

[16] J. Jirousek, A. Venkatesh. A new FE approach for adaptive reliability assurance. *Comp. Struct.*, **37**: 217–230, 1990.

[17] J. Jirousek. Structural analysis program SAFE – special features and advanced finite element models. *Adv. Eng. Software*, **7**: 68–76, 1985.

[18] J. Jirousek, A. Wróblewski, Q. Qin, X. He. A family of quadrilateral hybrid–Trefftz p–elements for thick plate analysis. *Comp. Meth. Appl. Mech. Eng.*, **127**: 315–344, 1995.

[19] A. Venkatesh, J. Jirousek. Accurate representation of local effect due to concentrated and discontineous loads in hybrid–Trefftz plate bending elements. *Comp. Struct.*, **57**: 863–870, 1995.